

ALD CONFORMALITY AND OPTIMIZATION IN ULTRAHIGH ASPECT RATIO NANOPORES FOR ELECTRICAL ENERGY STORAGE NANODEVICES

E.R. Cleveland^{1*}, L. Henn-Lecordier¹, I. Perez¹, P. Banerjee¹, and G.W. Rubloff²

¹Materials Science and Engineering Department, University of Maryland, College Park, USA

Abstract: In exploiting nanostructures for applications such as energy devices, conformal coatings are playing an increasingly crucial role. Atomic layer deposition (ALD) is receiving responsibility for the most demanding deposition in nanotechnology, especially in terms of conformality due to its self-limiting surface reactions. In this work, we investigate the effects of reactant dosage on deposition rates and thickness uniformity across a planar wafer versus conformality down the length of an ultrahigh aspect ratio nanopore as a means to optimize the ALD process in electrostatic nanocapacitor fabrication. Porous anodic alumina (PAA) templates were used as a versatile and facile platform to analyze TiO₂ ALD profiles via ex-situ SEM, EDS line scans and TEM. Initial results illustrate how tailoring precursor exposure times display CVD-like deposition mechanisms leading to poor conformality. These results provide insight to deposition mechanisms in ultrahigh aspect ratio nanostructures.

Keywords: atomic layer deposition, porous anodic alumina, ultrahigh aspect ratio, conformality

INTRODUCTION

Paralleling the trend in electronic devices, 3D architectures for applications such as energy devices [1], optoelectronics [2], catalysis [3], and various MEMS[4] and NEMS [5] devices are exploiting the benefits found in using nanostructures with increasingly high aspect ratios as well as nano-scale feature sizes. In exploiting these nanostructures, the 3D topography is perhaps even more complex and demanding than in conventional applications such as ULSI electronics, yet still demand highly conformal deposition processes. Atomic layer deposition (ALD) is replacing physical and chemical vapor deposition (CVD) methods due to their limited abilities to coat complex structures. ALD is widely accepted as a means to produce high quality films with atomic level thickness control and offers excellent thickness uniformity and conformality [6]. This control is inherent in the self-limiting surface chemistry where reactants are sequentially pulsed creating saturated chemisorbed surface reactions a monolayer at a time. In turn, ALD is used to create thin, dense, and pin-hole free films maintaining excellent electrical and optical properties even in demanding geometries.

As a vapor phase chemical deposition process, ALD differs from CVD in that it sequentially introduces gaseous precursors to a substrate's surface in a cyclic fashion preventing gas phase reactions. ALD is dependent on self-limiting surface reactions between a chemisorbed metal containing precursor and adsorbed nucleophilic reactants, such as [OH] surface species [6]. Therefore, one ALD cycle is described in four steps (Fig. 1): 1) exposure and

chemisorption of the first precursor, 2) inert gas purge removing excess of unreacted precursor, 3) introduction and surface reaction of the second precursor producing desired material, 4) inert gas purge removing reaction by-products. Ideally, if sufficient doses are applied to saturate a surface and purge times are adequate avoiding parasitic CVD-like reactions, one monolayer of film is deposited [7].

We are applying ALD to produce multilayer devices in nanopores with ultra-high aspect ratios (up to 1000:1) formed during anodic oxidation of aluminum to produce porous anodic alumina (PAA) [8]. The nanopores have diameters 15-100nm and depths 1-30 μ m, with uniform dimensions and spacing. As nanostructures are formed in the nanopores, extremely high conformality is required and becomes more demanding as the nanopore volume is increasingly filled to complete the structures.

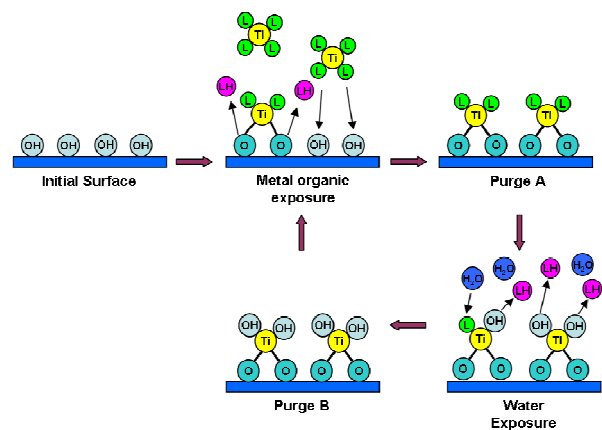


Fig. 1: Schematic of the cyclic alternating reactant exposures and purges during one TiO₂ ALD cycle.

To achieve precise control of nanostructure fabrication in a PAA membrane template, we have investigated the impact of key process metrics such as reactant dose on conformality profiles of ALD layers deposited into PAA nanopores, focusing on TiO₂ as a high-K insulator sought for ultrahigh density electrostatic nanocapacitors. While uniform films can be achieved across a planar wafer with the correct recipe of saturating doses and sufficient purge times, saturation doses and purge times become insufficient when translated to an ultra-high aspect ratio nanopore, caused by significantly larger surface areas to be covered and the interplay between diffusion and surface reaction within the nanopores [7]. We have adjusted ALD process recipes to optimize conformality in the nanopores while monitoring the consequences of higher precursor doses on across-wafer uniformity, anticipating that viable technologies will require conformal deposition profiles in nanopores across extended PAA substrates.

EXPERIMENTAL

PAA templates were synthesized using a two-step anodization process [8]. An electropolished sheet of aluminum was first anodized for ~8 hrs using 2.7wt% aqueous oxalic acid at 40V and 8 °C in order to produce hexagonally ordered pore arrays with interpore spacings of 105nm [8]. After the 1st anodization, the alumina film produced was removed in a mixture of phosphoric acid (6wt%) and chromic acid (1.8wt%) at 60 °C. This left the underlying aluminum surface pre-textured with an ordered hexagonal dimple array. The aluminum went through a 2nd anodization allowing pores to nucleate under each of the dimples in the surface, creating an ordered PAA array. Foils were anodized for ~14 min defining pores depths of ~10 μm. Pore diameters were adjusted to ~90 nm using a pore-widening solution of 1:1 NH₄OH.

High-k dielectric TiO₂ films were deposited in a custom built ultra-high vacuum (UHV) cross-flow wafer scale ALD reactor, using titanium tetraisopropoxide (TTIP) and ozone (O₃) as precursors. A 0.1L mini-reactor is embedded in the UHV process chamber equipped with a 100mm substrate heater and a pneumatically actuated stainless steel cap. Precursors and nitrogen gases are introduced and exhausted through 2 opposing slits positioned 3 mm above the wafer. The mini-reactor is operated at 130 mTorr and the substrate heater was maintained at 200 °C. TTIP doses were varied for 1, 3 and 6 μpulses, while ozone doses were maintained in an over-saturation regime. Purge times were

maintained at 20 sec between both precursors' half cycles.

TiO₂ films were deposited on both flat Si substrates and in PAA templates. Si samples were dipped in 3% HF solution to remove the native oxide and PAA templates were adhered to the Si near the inlet of the precursors. After deposition planar maps of film thickness and refractive index were obtained using a Sopra GES5 spectroscopic ellipsometer with an automated xy stage. Thickness profiles were taken of equidistant points across the wafer in the direction of the flow, with the first point being closest to the gas inlet and the last point being closest to the exhaust outlet. The percentage of non-uniformity is determined by the ratio of the standard deviation over the mean value (σ/μ) of all points taken across the wafer.

High resolution top down and cross sectional SEM was performed on bare and ALD coated PAA samples using a Hitachi SU-70 SEM equipped with EDS. Cross sectional PAA samples were made by removing the underlying aluminum and cleaving the remaining PAA membrane. EDS line scans were taken across the cleaved ALD deposited PAA templates. Film thickness as a function of pore length was extracted from the EDS compositional scans by setting the intensity proportional to the cylindrical volume of the sample being measured.

To confirm film conformality, 10 μm deep PAA templates were dissolved in 25% phosphoric acid to release TiO₂ nanotubes. Nanotubes were filtered and placed on a standard copper grid for TEM analysis using a JEOL 2100F with EDS capabilities.

DISCUSSION

TTIP doses were varied from an ideal planar saturation to an over-saturation level. In order to increase the dose and residence time of the metal precursor, doses were broken up and consecutively introduced as μpulses, where 1 μpulse of TTIP is 0.97 μmols. Fig. 2(a) shows across-wafer thickness profiles across planar Si substrates for 3 different TTIP doses and a fixed ozone dose. A TTIP dose consisting of 1 μpulse produced a uniform film (non-uniformity ~0.5%) with a reasonable growth rate of ~0.7 Å/cycle. However, Fig. 2(b) shows that as the number of μpulses increases the uniformity degraded and resulted in higher growth rates presenting CVD-like behavior due to insufficient purge times.

PAA templates with 10 μm deep pores and 90 nm diameters (aspect ratio ~100) were deposited in during the same runs for the planar Si samples. The data in Fig. 3(a) clearly show thickness gradients down the

length of the pore for each case. Initial deposition in the pore for the 1 μ pulse case show growth rates of 0.7 $\text{\AA}/\text{cycle}$ which are comparable to the planar case. However, growth rates decrease by 23% near the bottom of the pore. Initially this was believed to be due to insufficient doses or residence times for a molecule to diffuse down the length of the nanopore. However, as μ pulses were increased, growth rates near the pore entrance were significantly increased displaying CVD-like behavior.

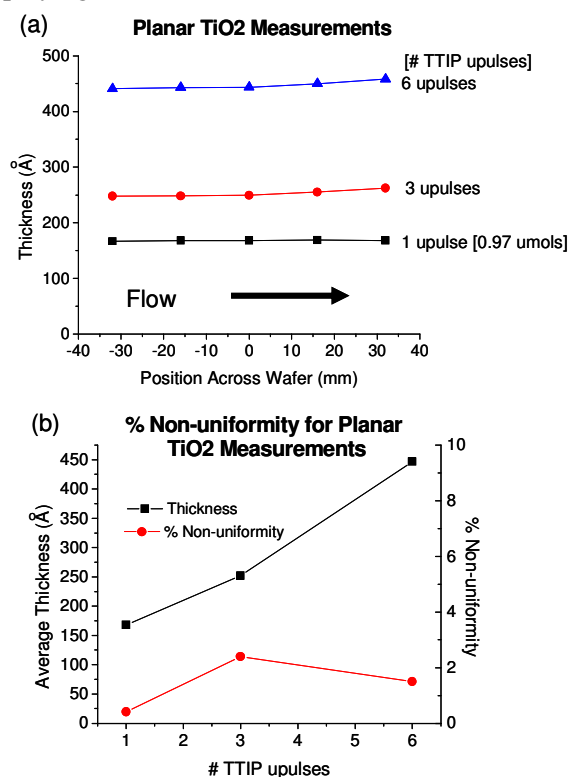


Fig. 2: (a) Across-wafer thickness profiles for 3 consecutive runs under a fixed ozone dose and varying the TTIP dose. 1 μ pulse is 0.97 μmol s. (b) Average thicknesses with corresponding planar % non-uniformity as a function of TTIP dose.

Fig. 3(b) shows the % non-conformality significantly increase as the number of TTIP μ pulses increase due to CVD-like behavior at the pore entrance. Due to this parasitic behavior the entrance to the pore closed faster than it would during ideal ALD. This means precursor doses became insufficient due to a lack of molecules that were able to diffuse down the length of the nanopore and react on an empty site; also purge times became insufficient to allow by products to be purged out of the nanopore before the next precursor was exposed.

Bright-field TEM allows 3D nanotubes to be imaged as a 2D projection so that darker areas indicate thicker or denser regions along the beam direction. Fig. 4 shows the bottom of a TiO_2 ALD

nanotube released by dissolving away the PAA template after ALD with 1 μ pulse of TTIP. Wall thicknesses of ~ 40 \AA taken near the bottom of the nanotube and are in good correlation to the EDS inferred thickness taken during cross-sectional SEM. Nanotube diameters were measured to be ~ 75 nm. The decrease in the nanotube diameter is due to an insufficient pore widening of the original PAA template. EDS line scans across the nanotube confirms the film is TiO_2 .

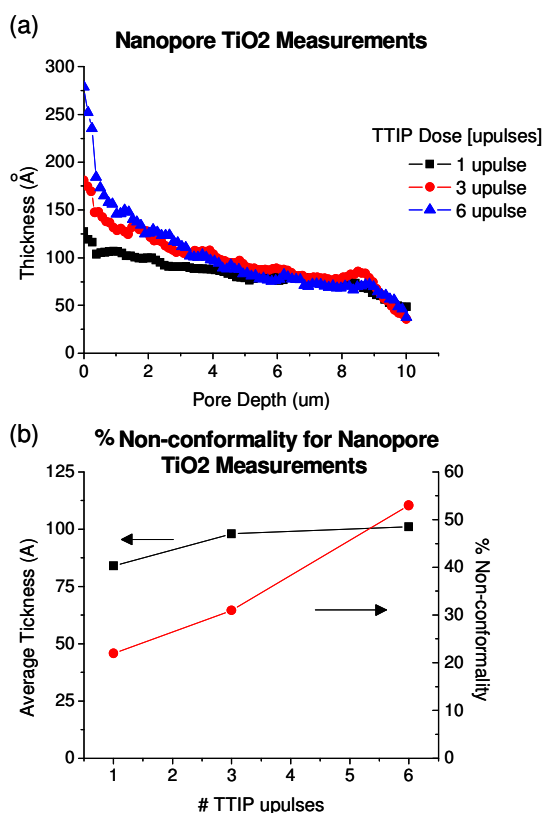


Fig. 3: (a) EDS inferred thickness profiles down the length of a ~ 10 μm deep pore for 3 consecutive runs under a fixed ozone dose and varying the TTIP dose. 1 μ pulse is 0.97 μmol s. (b) Average thicknesses with corresponding nanopore % non-conformality as a function of TTIP dose.

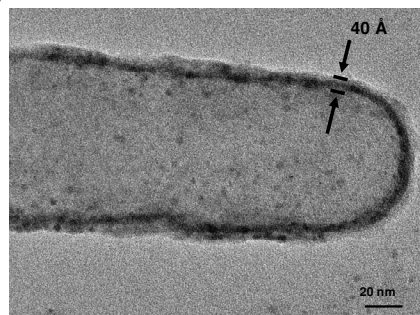


Fig. 4: TEM image of the bottom of a ~ 10 μm long TiO_2 ALD nanotube released from a PAA template after ALD using 1 μ pulse of TTIP and a fixed ozone dose.

CONCLUSION

ALD is receiving credit for some of the most demanding deposition in nanotechnology due to its exceptional ability to coat ultrahigh aspect ratio structures with very thin films. However, it has been demonstrated that maintaining atomic level thickness control with wafer scale uniformity *and* nanopore conformality is subject to the complex reaction dynamics associated with chemisorbed reactions. As shown across-wafer uniformity does not guarantee conformality down the length of a nanopore. However, further studies to optimize the ALD process for both uniformity and conformality as functions of process parameters, such as dose, purge, temperature and pressure are needed in order to preserve a material's desired properties (electrical, optical, compositional, etc.).

REFERENCES

- [1] P. Banerjee, Perez, I., Henn-Lecordier, L., Lee, S.B., Rubloff, G.W., 2009 Nanotubular metal-insulator-metal capacitor arrays for energy storage, *Nature Nanotechnology*, **4**, pp. 292-296.
- [2] J. S. King, D. Heineman, E. Graugnard, and C. J. Summers, 2005 Atomic layer deposition in porous structures: 3D photonic crystals, *Applied Surface Science*, **244**, pp. 511-516.
- [3] M. J. Pellin, P. C. Stair, G. Xiong, J. W. Elam, J. Birrell, L. Curtiss, S. M. George, C. Y. Han, L. Iton, H. Kung, M. Kung, and H. H. Wang, 2005 Mesoporous catalytic membranes: Synthetic control of pore size and wall composition, *Catalysis Letters*, **102**, pp. 127-130.
- [4] T. M. Mayer, J. W. Elam, S. M. George, P. G. Kotula, and R. S. Goeke, 2003 Atomic-layer deposition of wear-resistant coatings for microelectromechanical devices, *Applied Physics Letters*, **82**, pp. 2883-2885.
- [5] M. Kemell, M. Ritala, M. Leskela, R. Groenen, and S. Lindfors, 2008 Coating of Highly Porous Fiber Matrices by Atomic Layer Deposition, *Chemical Vapor Deposition*, **14**, pp. 347-352.
- [6] M. Leskela and M. Ritala, 2002 Atomic layer deposition (ALD): from precursors to thin film structures, *Thin Solid Films*, **409**, pp. 138-146.
- [7] S. O. Kucheyev, J. Biener, T. F. Baumann, Y. M. Wang, A. V. Hamza, Z. Li, D. K. Lee, and R. G. Gordon, 2008 Mechanisms of atomic layer deposition on substrates with ultrahigh aspect ratios, *Langmuir*, **24**, pp. 943-948.
- [8] H. Masuda and K. Fukuda, 1995 Ordered Metal Nanohole Arrays Made By a 2-step Replication of Honeycomb Structures of Anodic Alumina, *Science*, **268**, pp. 1466-1468.